REPORT DOCUMENTATION PAGE

Form Approved
OMB No. 0704-0188

PLEASE DO NOT RETURN YOUR FORM TO THE ABOVE ORGANIZATION.

1. REPORT DATE *(DD-MM-YYYY)*	2. REPORT TYPE	3. DATES COVERED *(From - To)*
1 Apr 2007	Final Performance Report	1 Apr 07-31 May 10

4. TITLE AND SUBTITLE
Development of a Nonlinear Cumulative Fatigue Damage Methodology for Aircraft Engine Components under Multiaxial Loadings

5a. CONTRACT NUMBER
FA9550-07-1-0270

5b. GRANT NUMBER

5c. PROGRAM ELEMENT NUMBER

6. AUTHOR(S)
Dr. Alan Kallmeyer

5d. PROJECT NUMBER

5e. TASK NUMBER

5f. WORK UNIT NUMBER

7. PERFORMING ORGANIZATION NAME(S) AND ADDRESS(ES)

Department of Mechanical Engineering
North Dakota State University

8. PERFORMING ORGANIZATION REPORT NUMBER

9. SPONSORING/MONITORING AGENCY NAME(S) AND ADDRESS(ES)
Air Force Office of Scientific Research
875 North Randolph Street
Arlington, VA22203

10. SPONSOR/MONITOR'S ACRONYM(S)

11. SPONSOR/MONITOR'S REPORT
AFRL-OSR-VA-TR-2013-0980

12. DISTRIBUTION/AVAILABILITY STATEMENT
Distribution Statement A: Approved for public release. Distribution is unlimited.

13. SUPPLEMENTARY NOTES

14. ABSTRACT
This report summarizes the results of a study focusing on the development of a robust methodology for cumulative fatigue damage analysis of aircraft engine alloys. This effort consisted of an experimental component and an analytical component. The experimental test program was designed to provide critical information related to damage accumulation, including effects such as multiaxiality of the stress field and LCF/HCF interactions. A new critical-plane based multiaxial fatigue damage parameter was proposed that provided good correlation with experimental test data. Finally, a nonlinear cumulative damage model was developed, based on the damage curve concept, that accounts for load-sequence and load-interaction effects, as well as damage caused by sub-threshold HCF cycles.

15. SUBJECT TERMS

16. SECURITY CLASSIFICATION OF:			17. LIMITATION OF ABSTRACT	18. NUMBER OF PAGES	19a. NAME OF RESPONSIBLE PERSON
a. REPORT	b. ABSTRACT	c. THIS PAGE			19b. TELEPHONE NUMBER *(Include area code)*

Development of a Nonlinear Cumulative Fatigue Damage Methodology for Aircraft Engine Components under Multiaxial Loadings

Final Report

FY 2007 T&E Research Program
Grant Number: FA9550-07-1-0270

PI: Dr. Alan Kallmeyer
Department of Mechanical Engineering
North Dakota State University

Introduction and Background

Many turbine engine components are subjected to complex loadings in service that vary in direction and intensity. Accurate and reliable life predictions for such components require methodologies that can assess the damage caused by individual load events and provide a means for estimating the accumulation of damage under realistic loading scenarios. The consideration of important contributing factors, including multiaxiality of the stress field, interactions between LCF and HCF loads, and the rate of damage accumulation under variable loading conditions, presents challenges in the development of a robust, yet useable design methodology. Consequently, most component and system lifing procedures currently in use have adopted simplifying assumptions, coupled with experimental verification through elaborate component and engine testing regiments, to establish durability limits for aircraft engines.

Despite a substantial body of research showing that the accumulation of fatigue damage in metals is dependent on several factors, including load sequence, load path, and load interactions, the Palmgren-Miner linear damage rule (Miner's rule) is still used almost exclusively in commercial fatigue life prediction algorithms. Although it is generally recognized that the linear damage assumption may lead to inaccuracies, it is utilized for its computational simplicity and due to the widespread recognition that there are no other proven methodologies capable of providing consistently better results. Numerous nonlinear cumulative damage models have been proposed in the technical literature. However, these models have generally been derived in response to specific phenomena observed under limited experimental test programs, most notably under uniaxial loading conditions. Such models, while often showing good correlation to a specific data set, have not demonstrated any widespread ability to model fatigue damage accumulation under a variety of loading conditions. These models are, for the most part, empirical approaches that have relied little on analytical considerations of the causes of nonlinear damage accumulation.

Previous studies performed by the PI [1 – 3], demonstrated that fatigue damage accumulation in aircraft engine materials is highly sensitive to load path (multiaxiality), load-level (LCF/HCF) and load-path interactions among cycles in the history, and the relative amounts of LCF damage and HCF damage in the load history. Thus, a robust lifing methodology for turbine engine components must incorporate the following:

- A multiaxial fatigue damage parameter capable of accurately predicting fatigue lives under a variety of loading conditions, including non-proportional loadings and multiaxial mean stresses, over a range of levels spanning LCF to HCF loadings. This parameter must be developed based on a physical interpretation of the damage mechanisms so that it possesses the capability to distinguish between the different damage mechanisms responsible for the nucleation and growth of small cracks in the LCF and HCF regimes.
- A means for defining and identifying individual load cycles within a multiaxial, variable load sequence. While accepted cycle-counting procedures have long been recognized for uniaxial load sequences, the extension to multiaxial loadings brings forth additional challenges, particularly when stress components cycle out of phase of one another.
- A cumulative damage rule capable of accounting for load-sequence effects, load interactions among LCF and HCF cycles, and nonlinear damage accumulation rates that are dependent on the degree of LCF and HCF damage in the service history.
- Finally, the methodology must be easily implemented and adaptable to current lifing algorithms that are utilized by design engineers.

This report summarizes the results of a study focusing on the development of a robust methodology for cumulative fatigue damage analysis of aircraft engine alloys. This effort consisted of an experimental component and an analytical component. The experimental test program was designed to provide critical information related to damage accumulation, including effects such as multiaxiality of the stress field and LCF/HCF interactions. A new critical-plane based multiaxial fatigue damage parameter was proposed that provided good correlation with experimental test data. Finally, a nonlinear cumulative damage model was developed, based on the damage curve concept, that accounts for load-sequence and load-interaction effects, as well as damage caused by sub-threshold HCF cycles. The details of the experimental and analytical results are provided in the following sections.

Experimental Results: Multiaxial Fatigue Tests

A total of 62 multiaxial fatigue specimens were machined from forged plates of Ti-6Al-4V. This material was chosen for analysis because it is commonly used in aircraft turbine engines, is readily available, and has been well characterized. Both tubular (hollow) and solid specimens were utilized in this study. Thin-walled tubes are preferred for tension/torsion tests due to the simplified analysis that results from the assumption of constant shear stress through the tube walls. Provided the applied loads are not too large, as is typical of HCF loading conditions, thin-walled tubes can be safely tested in tension/torsion. However, when subjected to higher loads representative of LCF conditions, there is a concern of thin-walled buckling in torsion. Consequently, several biaxial LCF tests were conducted using solid specimens.

The test section for the tubular specimens had a nominal OD of 0.375 in and ID of 0.25 in, and a length of 1.5 in. The solid specimens had a nominal test section diameter of 0.5 in and length of 1.2 in. All specimens were subjected to a low stress grind to 16 RMS, and then longitudinally polished to 8 RMS. A total of 52 tubular specimens and 12 solid specimens were machined.

All multiaxial fatigue tests were performed at the Structural Integrity Laboratory at the University of Utah, under the direction of Dr. Dan Adams and Jeff Kessler, and the Advanced

Materials Testing Laboratory at the University of Illinois, under the direction of Dr. Peter Kurath. The LCF tests were conducted in strain control due to the high level of yielding along the outer surface of the specimens. The HCF tests, which experienced very low levels of plastic behavior, were conducted under load-control conditions. An elastic-plastic finite element analysis was performed to determine surface stresses in specimens that incurred plastic strains at the peak load level.

Several constant-amplitude biaxial fatigue tests were first performed to assist in the development of the multiaxial fatigue damage parameter, as well as to calibrate the final model. These tests consisted of uniaxial, torsion, and proportional tension/torsion tests at stress ratios of $R = -1$ and $R = 0$. Load levels were varied to produce fatigue lives covering the spectrum from LCF to HCF conditions. The results of the constant-amplitude tests are listed in Appendix 1. The elastic-plastic stresses listed in this table represent the surface stresses at maximum and minimum loads as determined by an elastic-plastic finite element analysis using ANSYS.

Next, a series of simulated "mission" tests were conducted, consisting of a mix of LCF and HCF cycles with varying load paths. These tests were conducted to analyze the effects of load-path and load-level interactions. The load paths used in this phase of the test program were the same as those used in the constant-amplitude tests. However, the types of load paths were varied between LCF and HCF cycles in order to create differing relationships in damage mechanisms among the cycles in these tests. The intent was to better understand how variations in load path between cycles affect the rate of damage accumulation under multiaxial loading conditions.

All multiaxial mission tests were comprised of a block of cycles consisting of 1 LCF cycle coupled with 50 HCF cycles, as illustrated schematically for uniaxial loading conditions in Fig. 1. In all cases, LCF lives were on the order of 10^5 cycles, while HCF levels were at or below threshold levels (infinite life conditions). Thus, on the basis of a conventional linear cumulative damage analysis, the HCF cycles would contribute no damage, meaning the mission lives would be expected to be similar to LCF lives. The load paths used in these tests are illustrated schematically in Fig. 2. The test conditions and results are listed in Appendix 2.

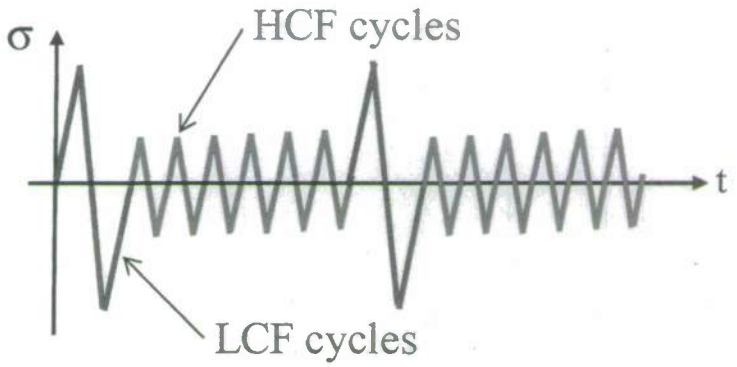

Figure 1. Schematic illustration of mission histories.

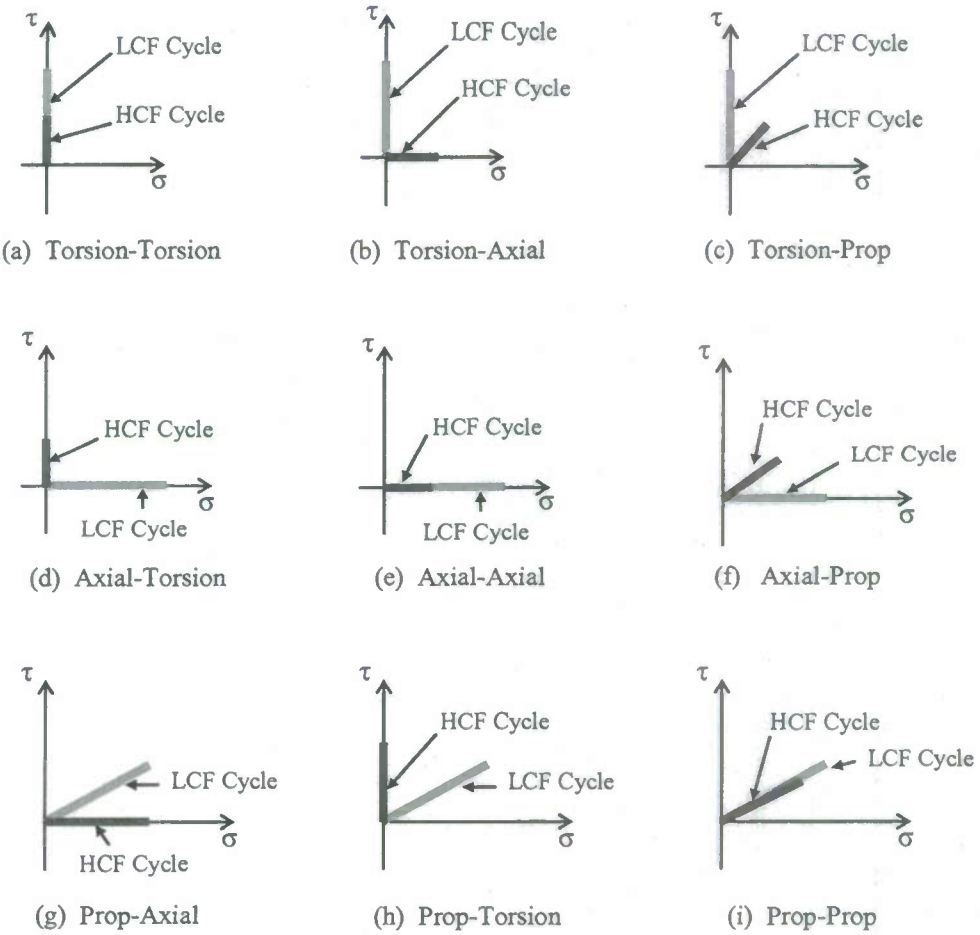

Figure 2. Multiaxial load paths used in the mission histories.

As previously noted, stress and strain values on the surface of the specimens experiencing yielding were determined from an elastic-plastic finite element analysis using ANSYS. This analysis employed a multilinear kinematic hardening rule in conjunction with the Ramberg-Osgood cyclic stress-strain curve, as measured from strain-controlled uniaxial tests. This curve is shown in Fig. 3, along with the experimental data. The material parameters for the Ramberg-Osgood formulation, shown in Eq. (1), were found to be E = 111.8 GPa, K' = 1383 MPa, and n' = 0.0956.

$$\varepsilon = \frac{\sigma}{E} + \left(\frac{\sigma}{K'}\right)^{1/n'} \tag{1}$$

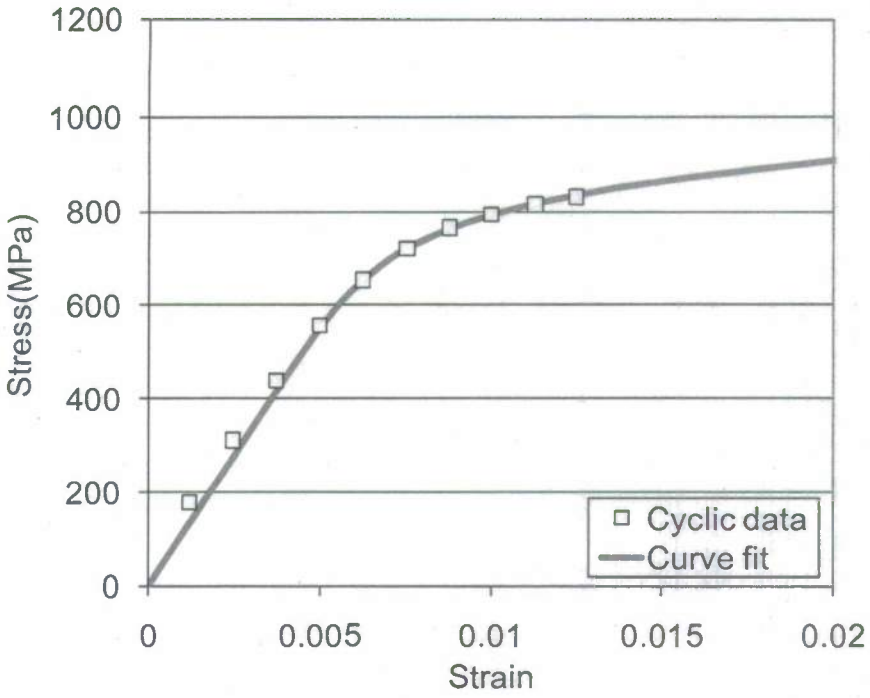

Figure 3. Cyclic stress-strain curve.

The results of the mission tests are presented graphically in Fig. 4, relative to the corresponding LCF tests. This figure plots the mission lives (square symbols) in relation to the LCF lives (circles) for a variety of load paths (tensile, torsion, and proportional). As is evident from these results, the presence of very small HCF cycles in a load history caused a substantial reduction in the mission lives, relative to LCF lives, in some cases. Notably, some mission lives were reduced by a factor of 20 or more due to the HCF cycles; however, the life reductions were heavily dependent on the load path relationships between the LCF and HCF cycles. Conventional damage accumulation techniques, such as those based on the Palmgren-Miner linear damage rule, would thus drastically overestimate the mission lives. These results indicate a pressing need to develop more accurate life prediction techniques for variable amplitude loading that take into account nonlinear damage accumulation and load path interactions.

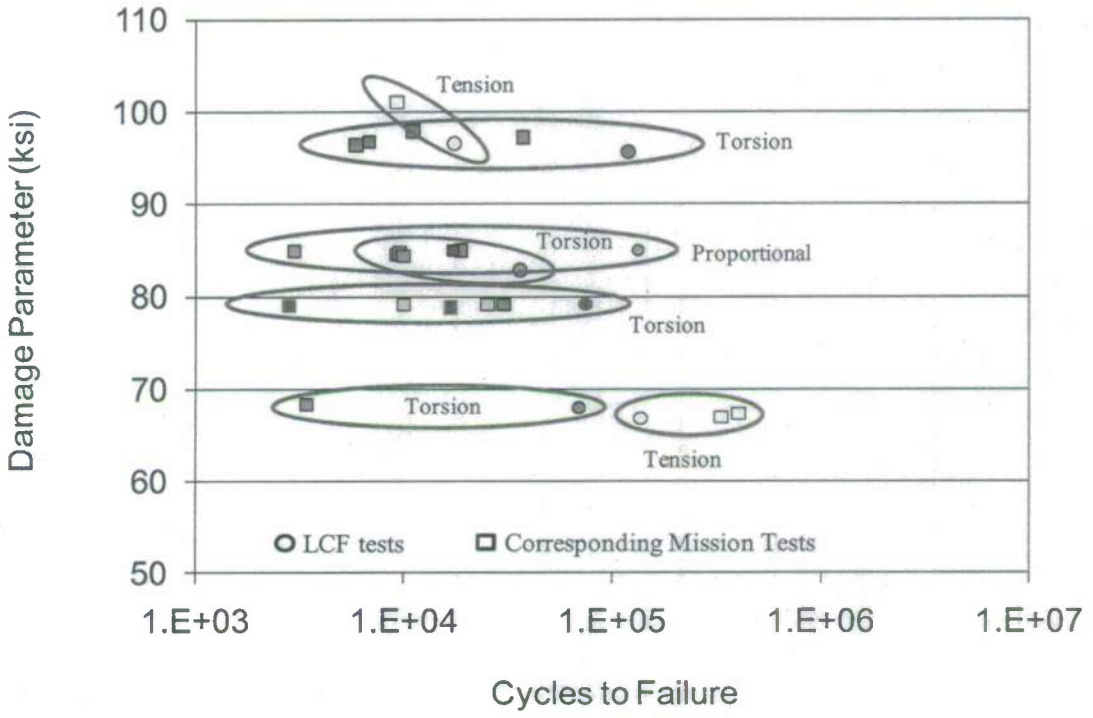

Figure 4. Comparison of mission lives and LCF lives.

Multiaxial Fatigue Modeling: Critical Plane Analysis

The approach taken in this study for cumulative damage analysis of aircraft engine components focuses on the nucleation and growth of small cracks (microcracks), rather than the propagation of macrocracks. Many engine components are currently life-limited on the basis of crack nucleation, as this typically consumes the majority of the total life under the loading conditions to which these components are subjected. Since a requirement of the damage accumulation model is that it be easy to use by a design engineer, it is important that this model be capable of being integrated within existing design algorithms. Furthermore, the effect of load multiaxiality on crack growth appears to be less of a concern than on crack nucleation. Many researchers have reported that, under mixed-mode loading, macrocracks tend to grow predominantly under mode-I conditions. In addition, conventional analysis techniques for crack growth, based on fracture mechanics principles, inherently account for nonlinearity in damage growth and load-sequence effects through an incremental crack propagation analysis that can model crack retardation due to overloads using crack closure and plastic zone concepts. Conversely, for crack nucleation, there are no broadly applicable techniques currently available for cumulative damage analysis other than Miner's rule, despite overwhelming experimental evidence of nonlinear damage accumulation. Thus, the focus of this study was to provide a mission-based lifing methodology for engine components based on crack nucleation concepts

that accounts for multiaxial stress states and nonlinear damage accumulation, and which can be implemented into existing design codes.

Past research by the PI [4] resulted in the development of a critical-plane parameter for crack nucleation that demonstrated an excellent ability to correlate uniaxial and multiaxial (tension/torsion) fatigue data for aircraft engine alloys, including Ti-6Al-4V. This parameter was expressed as

$$DP = \tau_{\max}\left(1-\frac{\tau_{\min}}{\tau_{\max}}\right)^{w_1}\left(1+\frac{k_1\sigma_{\tau\max}+k_1\sigma_{\tau\min}}{\sigma_y}\right)+k_2\sum\sigma^{+}_{\max}\left(1-\frac{\sigma^{+}_{\min}}{\sigma^{+}_{\max}}\right)^{w_2} \qquad (2)$$

$$\text{where } k_1 = \begin{cases} k_1^{+} \text{ if } \sigma > 0 \\ k_1^{-} \text{ if } \sigma < 0 \end{cases}$$

In Eq. (2), τ_{max} and τ_{min} are the shear reversal points on the critical plane (defined here as the plane of maximum alternating shear stress), and $\sigma_{\tau max}$ and $\sigma_{\tau min}$ are the corresponding normal stresses on this plane at the instant of shear reversal. These stresses are divided by the yield strength, σ_y, to maintain consistency of units. In the second term, σ_{max} and σ_{min} are the maximum and minimum normal stresses on the critical plane over the entire cycle. The σ^+ notation indicates that only positive (tensile) values are used in the equation. If σ_{min} or σ_{max} is negative, that value is set to zero in Eq. (2).

The derivation of this parameter was based on a physical interpretation of the mechanisms governing the nucleation and growth of small fatigue cracks. The first term in Eq. (2) represents the primary mechanism for crack nucleation in ductile metals; i.e., cyclic shear stresses. The form of the expression allows for the possibility of a mean shear stress effect, which has been observed in several aircraft engine alloys. The multiplier term (containing $\sigma_{\tau max}$ and $\sigma_{\tau min}$) acts to modify the shear component to account for crack face interaction due to the normal stresses at the shear reversals. A tensile normal stress will hold the crack open, reducing crack face interaction and friction, thereby accelerating crack advance along the shear plane. Conversely, a compressive normal stress will increase crack face interaction and friction, inhibiting the advance of the crack. The definition of the k_1 term allows for a different influence of tensile and compressive stresses. The last term in Eq. (2) accounts for the additional damage caused by cyclic tensile stresses on the critical plane. If multiple normal stress cycles exist within the shear cycle, their contribution is included through the summation in this term. The values of k_1, w_1, k_2 and w_2 are fit by collapsing uniaxial and multiaxial fatigue data.

A key aspect inherent in the damage parameter presented in Eq. (2) is the potential to distinguish between different damage mechanisms (e.g., shear vs. tensile). Prior work by the PI has shown a change in damage mechanisms between LCF and HCF cycles under multiaxial load paths, which may contribute to the highly nonlinear rates of damage accumulation observed in this study. In order to accurately model such effects, it is necessary to interpret the damage mechanisms between cycles and the potential for load-cycle interactions. The parameter in Eq. (2) separates fatigue damage into shear and tensile modes; however, there are drawbacks associated with this parameter that render it unsuitable for more complex variable load histories. For example, if multiple normal stress cycles exist *within* a single shear cycle, the summation on the last term may overestimate the damage associated with the major cycle. Hence, it is

necessary to break this damage term out independently and account for it within the cumulative damage model. In this manner, the model will not only allow for nonlinear damage accumulation from cycle to cycle, but also within an individual cycle due to different damage mechanisms. Furthermore, the separation of damage mechanisms on the critical plane allows the ability to weight the importance of those mechanisms differently in accordance with observed phenomena; e.g., shear mechanisms dominate within LCF cycles while tensile mechanisms dominate within HCF cycles.

In consideration of the issues presented above, along with a critical examination of constant amplitude multiaxial fatigue data generated in this study and previous studies by the PI, a new critical plane parameter was developed for LCF loadings. This parameter is shown in Eq. (3).

$$DP = (\tau_{max})^{1-w}(G\Delta\gamma)^{w} + k\frac{(\tau\sigma)_{max}}{\sigma_0} \tag{3}$$

In this equation, $\Delta\gamma$ is the shear strain range on the critical plane (defined as the plane of maximum cyclic shear stress/strain), τ_{max} is the maximum absolute value of shear stress on this plane (which allows the model to account for a mean shear stress effect), $(\tau\sigma)_{max}$ is the maximum product of shear and normal stress on the critical plane, σ_0 is an arbitrary reference stress value (to maintain unit consistency), G is the shear modulus, and w and k are material parameters determined from fitting experimental data. The last term in this equation is designed to account for the influence of the normal stress on the critical plane. A tensile normal stress will open the crack, thereby reducing crack face interaction and allowing the crack to nucleate more easily by the cyclic shear stress. However, this process is also dependent on the phase of the stresses; i.e., when a tensile normal stress occurs in-phase with a large shear stress, it will have a greater influence than if it occurs out-of-phase with the shear stress.

The new parameter shown in Eq. (3) has several advantages over the previous form shown in Eq. (2). The inclusion of the cyclic shear strain, $\Delta\gamma$, rather than just stress terms, allows the parameter to better model cyclic hardening or softening that often occurs under LCF loading. In addition, the absence of the summation of small cycle damage within the dominant shear cycle negates the overestimation of this type of damage that plagued the previous parameter. Instead, the contribution of small cycle (HCF) damage can be assessed independently in the cumulative damage model. Finally, the reduction of material parameters (from four to two) that must be fit from experimental data results in a much simplified model.

The new critical-plane parameter shown in Eq. (3) was fit to the constant-amplitude multiaxial fatigue data for Ti-6Al-4V generated in this study, presented in Fig. 5. As shown, there is a large variety of test data, including uniaxial, torsion, and proportional load paths tested under load-control and strain-control conditions. From this analysis, the following material parameters were obtained: σ_0 = 689 MPa, w = 0.46, and k = 0.8. Although there is a significant amount of scatter in the experimental fatigue data, it is evident that this parameter collapses the multiaxial data well, resulting in a simple and effective critical-plane model for the purposes of LCF life prediction of high-strength alloys subjected to multiaxial loading conditions.

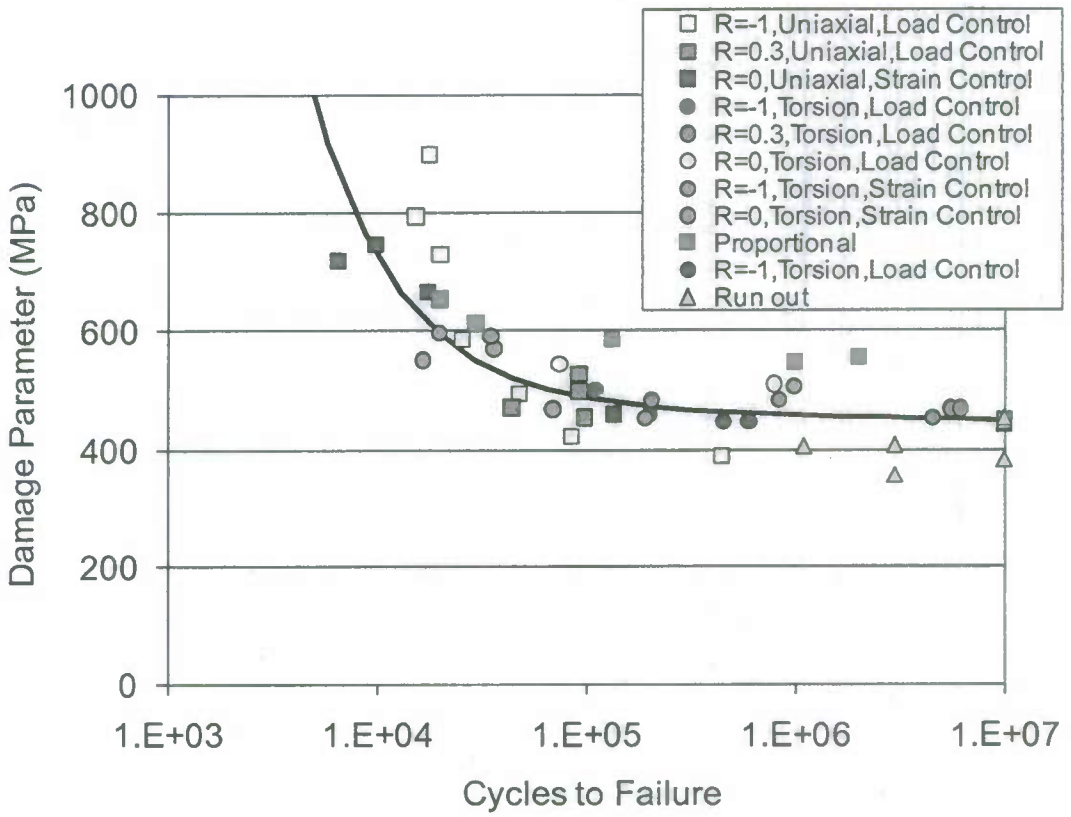

Figure 5. New damage parameter applied to multiaxial fatigue data for Ti-6Al-4V.

It is theorized here that the observed reduction in mission life due to the HCF cycles is caused by the propagation of microcracks initiated by the LCF cycles. As it is well known that crack propagation is driven primarily by cyclic tensile stresses, a tensile-stress based damage parameter will be required to model the additional damage caused by the HCF stresses. In this study, a Walker-type parameter was used for this purpose. The Walker parameter assumes that cyclic tensile stresses cause fatigue damage, and accounts for a mean stress effect through a modification incorporating the stress ratio and an adjustable material parameter, w. The form of the Walker parameter utilized in this study is shown in Eq. (4).

$$DP = \sigma_{max}\left(1 - \frac{\sigma_{min}}{\sigma_{max}}\right)^{w} \tag{4}$$

In order to develop a functional relationship for modeling the damage caused by the HCF cycles, the Walker parameter shown in Eq. (4) was fit to the uniaxial fatigue data generated in this study. The resulting curve fit is shown in Fig. 6 with w = 0.35. As is evident, the Walker parameter provides a good representation of the uniaxial (tensile) fatigue data, accounting for the effect of mean stresses. From this figure, it can be seen that values of the Walker parameter below approximately 700 MPa (100 ksi) would not be expected to contribute significantly to fatigue damage. Thus, a value of 700 MPa was used in subsequent analyses as a "threshold" value for fatigue damage contributions.

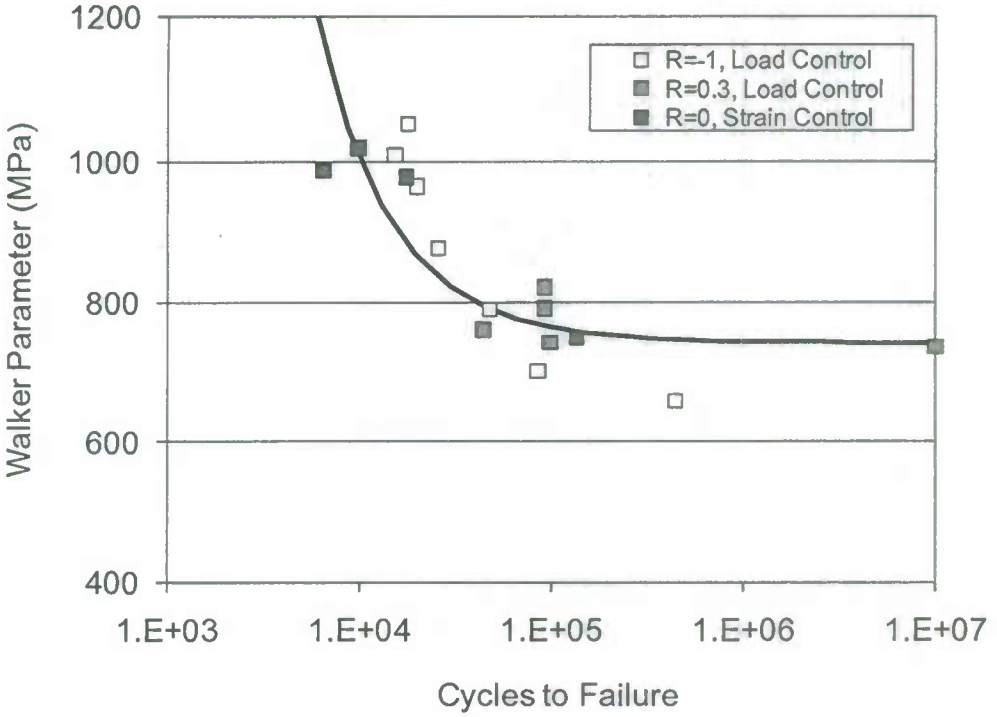

Figure 6. Walker parameter applied to uniaxial fatigue data for Ti-6Al-4V.

Nonlinear Damage Accumulation Model

Numerous empirical theories have been proposed to model nonlinear fatigue damage accumulation [5]. Among these models, the Damage Curve Approach (DCA), developed by Manson, Halford, and coworkers [6 – 7], has received greater attention due to its simplicity in application and its ability to account for several observed phenomena. In this model, the rate of damage accumulation is dependent on the load level (or equivalently, life to failure at that load level) and the life fraction, n/N_f. Thus, different damage curves govern the damage growth at different life levels. The rate of damage accumulation is assumed to increase as the number of applied cycles increases, and the degree of nonlinearity is greater at higher life levels (lower loads). Using this model, the instantaneous state of fatigue damage is calculated as

$$D = \left(\frac{n}{N_f}\right)^{\left(\frac{N_f}{N_{ref}}\right)^{\alpha}} \tag{5}$$

where α is a material parameter and N_{ref} is the life level at which damage accumulates linearly, generally taken as unity. The model is shown schematically in Fig. 7, illustrating how damage would be computed for a three-level block loading history in which the load levels are decreasing.

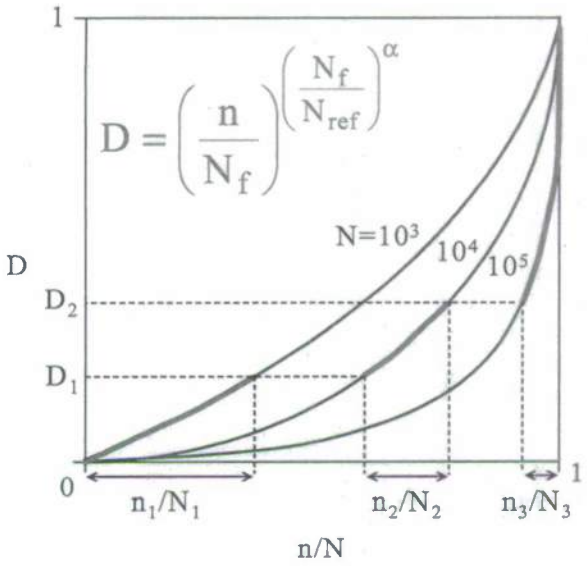

Figure 7. Illustration of the Damage Curve Approach.

A desirable feature of this model is that it captures the load-sequence effect commonly observed in two-level block loading tests. In addition, since the damage is expressed solely in terms of the fatigue life and life ratio, it is independent of the damage parameter used in the calculation of fatigue life once α has been obtained. However, a limitation of this model is that it neglects any damage caused by cycles below threshold or endurance values; i.e., if $N_f = \infty$, $D = 0$. Thus, for the tests conducted in this study (in which the HCF cycles were below threshold values), the model would predict no reduction in mission life due to the HCF cycles.

Due to the limitations of the DCA model, a new nonlinear damage accumulation model was developed through a modification to the original form. The primary objective was to allow the model to capture the damage contributions from very small HCF cycles, even those below threshold stress (endurance) limits. In this analysis, the sub-threshold HCF cycles are assumed to cause no damage unless prior damage has occurred, such as through the application of LCF cycles. Thus, in the absence of existing damage, the HCF cycles will cause no fatigue damage; i.e., these cycles are too small to nucleate fatigue cracks by themselves. However, if fatigue cracks are nucleated through LCF cycles, the HCF cycles will then contribute to the further development and growth of the microcracks.

In the model, this is accomplished by defining a "threshold" damage value, D_{th}, for small HCF cycles. This threshold value may vary with different HCF cycle levels. As long as the total accumulated damage (D) from prior cycles remains below D_{th}, a given HCF cycle will not contribute additional damage. However, once the total accumulated damage from prior cycles exceeds D_{th}, the associated HCF cycles will start to contribute damage.

The modified DCA model is illustrated in Fig. 8. In this figure, the blue lines represent finite-life damage curves; i.e., curves associated with LCF cycles corresponding to a specific fatigue life. The red lines represent damage curves associated with sub-threshold HCF cycles of varying magnitudes, resulting in different D_{th} values for each load level. Whereas the LCF cycles may start to accumulate damage immediately, the HCF cycles will not contribute damage until the corresponding D_{th} value has been surpassed. Smaller HCF cycles have higher D_{th} values than larger HCF cycles, but eventually all cycles will contribute damage.

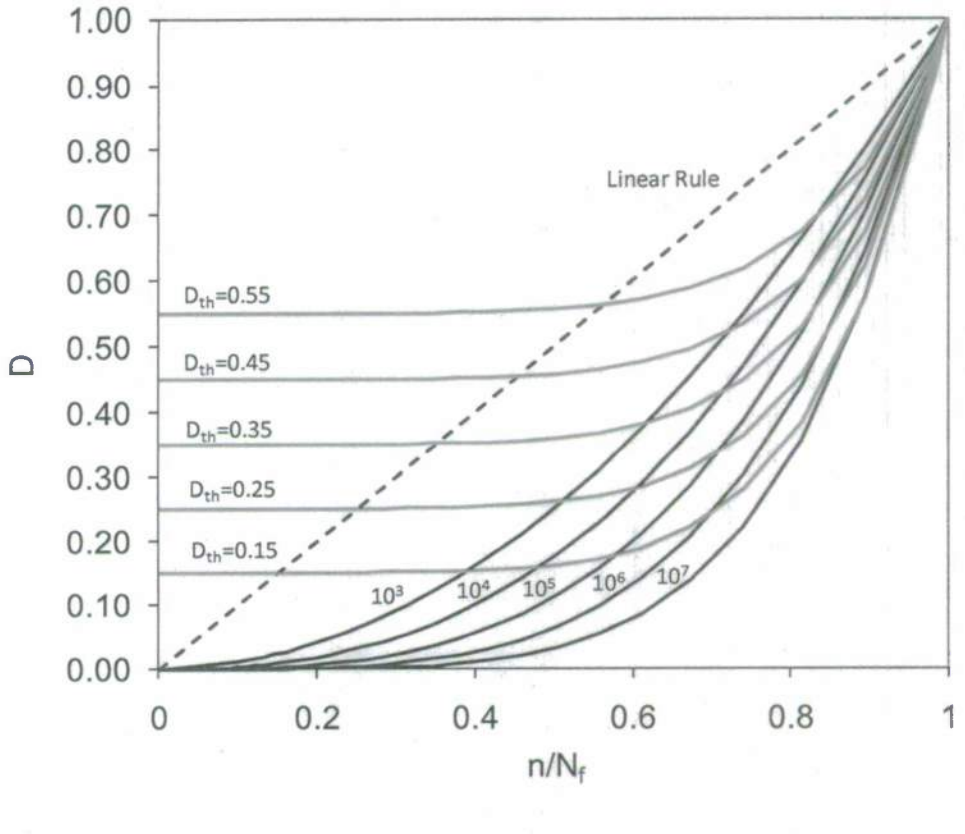

Figure 8. Illustration of the modified Damage Curve Approach.

Mathematically, the damage function for the new model is expressed as

$$D = D_{th} + (1 - D_{th}) \times \left(\frac{n}{N_f}\right)^{(N_f)^{\alpha}} \tag{6}$$

where the threshold damage value, D_{th}, is given in terms of the threshold damage parameter value (e.g., endurance limit), DP_{th},

$$D_{th} = \left(1 - \frac{DP}{DP_{th}}\right)^{\beta} \tag{7}$$

In using these equations, if the current value of the damage parameter (DP) exceeds DP_{th}, then $D_{th} = 0$ and D is calculated directly from Eq. (6). However, if $DP < DP_{th}$, then D_{th} is first calculated from Eq. (7), with D subsequently determined from Eq. (6). The constants α and β are considered material parameters that must be fit from experimental data. They govern the degree of nonlinearity inherent in the accumulation of fatigue damage. A desirable feature of this model is that different damage parameters can be used for different types of cycles to better model different damage mechanisms that may occur between cycles; e.g., LCF vs. HCF damage mechanisms.

The modified DCA model was applied to the results of the mission histories tested in this study. In this analysis, the shear-based damage parameter shown in Eq. (3) was used for the LCF cycles, while the tensile-based Walker parameter shown in Eq. (4) was used for the HCF cycles. Based on the results shown in Fig. 6, a value of 700 MPa was used for the HCF DP_{th} value in Eq. (7). Optimal values of α and β were determined for each test by matching experimental and predicted lives, then these values were averaged to determine a single, optimal value of each constant for the Ti-6Al-4V material. From this process, the following values were determined: $\alpha = 0.25$, $\beta = 0.5$.

Several damage curves for the Ti-6Al-4V material using the aforementioned material parameters are shown in Fig. 9. As before, the blue curves represent finite-life (LCF) damage curves, for which the damage parameter is calculated from Eq. (3). The red curves represent HCF damage, for which the damage parameter is calculated from Eq. (4). In these cases, the DP values are less than the threshold value of 700 MPa, requiring the use of both Eqs. (6) and (7) to calculate the current damage level.

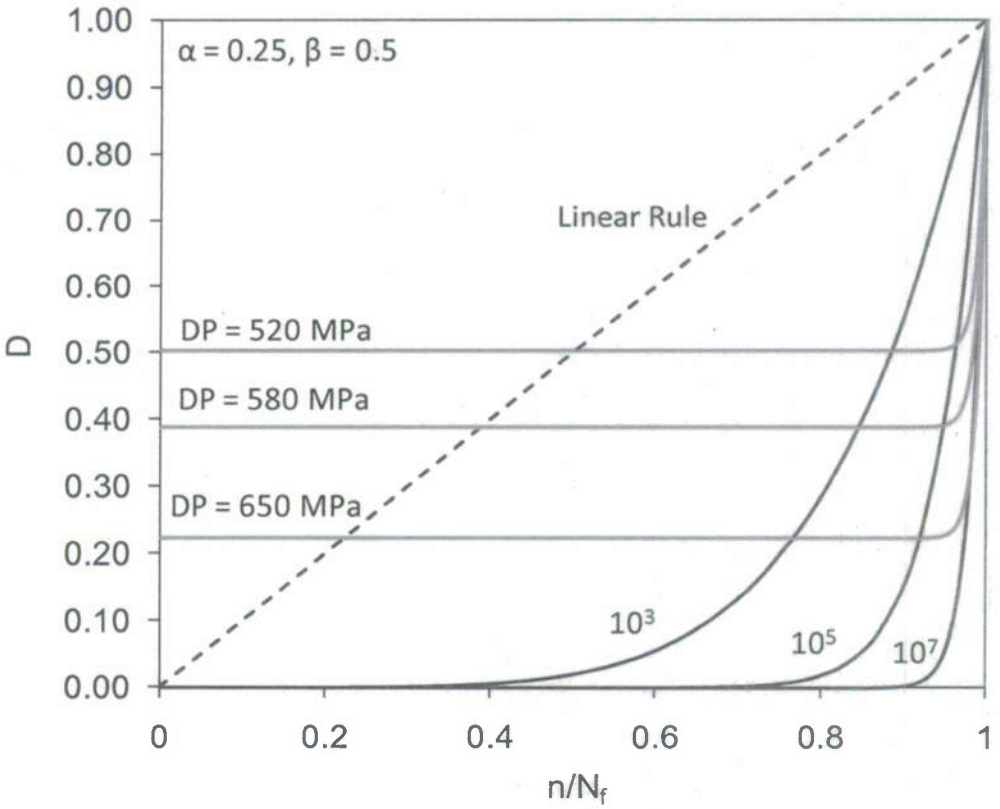

Figure 9. Damage curves for Ti-6Al-4V. DP values shown refer to sub-threshold values of the Walker parameter.

Using the new damage model, predicted lives were calculated for the mission histories tested in this study, and compared to the experimental lives. The results are shown in Fig. 10 in the form of a predicted vs. experimental life plot. The corresponding predictions using the linear damage rule are also included for comparison. In this plot, the solid lines on either side of the main diagonal represent a scatter band of a factor of two in the life predictions, while the dashed

lines represent a factor of ten scatter band. It is clear that in nearly all cases, the linear rule was highly non-conservative, with predicted lives often exceeding experimental lives by a factor of 10 or more. In only two cases did the linear damage rule provide accurate life predictions within a factor of two of the experimental lives. In contrast, the proposed nonlinear damage model resulted in all life predictions falling within a factor of ten, and half of the predictions falling within a factor of two of experimental lives. Thus, the new model presents a clear improvement in estimating the fatigue damage caused by small cycles, as well as accounting for the load-path interactions between LCF and HCF cycles through consideration of the varying stress states on the critical plane.

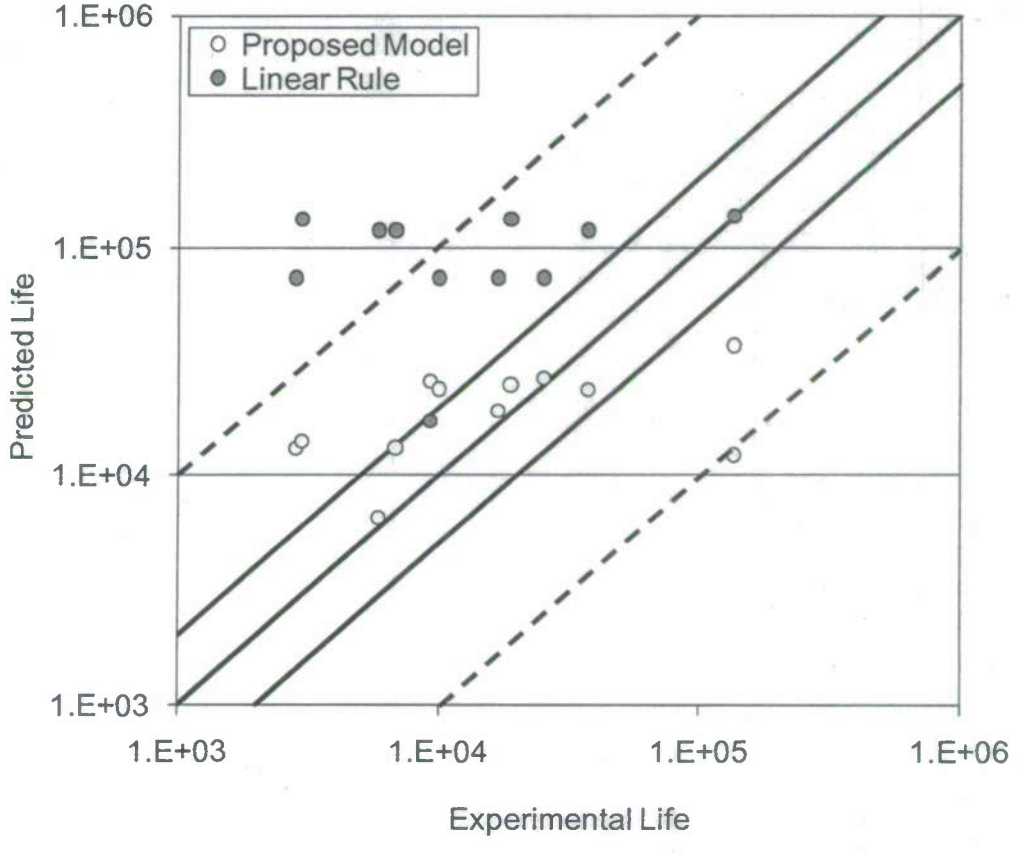

Figure 10. Predicted vs. experimental lives for the mission tests using the new damage model. Life predictions are also shown using the conventional linear damage rule.

Summary

A comprehensive study was undertaken to investigate and model the accumulation of fatigue damage under multiaxial loading, with an emphasis on LCF/HCF interactions, load-path dependence between large and small cycles, and nonlinear rates of damage accumulation. Experimental testing revealed a very strong effect on damage accumulation from HCF cycles, even those that would typically be considered below threshold or endurance levels. However, the influence of the HCF cycles is heavily dependent on the load path. Notably, load histories in

which cyclic tensile stresses from HCF cycles are maximized on or near LCF critical shear planes appear to exhibit significant damage interactions. Also, there is a substantial influence from HCF cycles in torsional loading. However, under uniaxial loading conditions, the effect of the HCF cycles was found to be negligible. This is an important point, as most fatigue damage studies have utilized primarily uniaxial test data.

Based on the experimental evidence, a new approach to modeling fatigue damage accumulation was presented. The approach relies on a multiaxial critical plane analysis to identify the plane of crack nucleation from the LCF cycles, assumed here to be shear dominated. A separate parameter, based on tensile stresses, is used to assess the damage caused by HCF cycles on the LCF critical plane. The rate of damage accumulation is assumed to be nonlinear, and dependent on the life (load) level of each cycle. A "threshold damage" level was introduced for HCF cycles. When the accumulated damage is below the threshold level for any given cycle, that cycle is assumed to cause no damage. However, once exceeded (such as from larger cycles), even very small cycles can contribute to fatigue damage accumulation. The new model was used to predict fatigue lives of simulated mission histories tested in this study, and the results were found to be significantly improved over the traditional linear damage rule. Hence, this new approach provides a more reliable way to assess fatigue damage accumulation in metals than most current methodologies, specifically accounting for multiaxial loadings and LCF/HCF interactions.

References

1. Goodin, E., Kallmeyer, A.R., and Kurath, P., "Cyclic Event Identification and Fatigue Damage Assessment for Multiaxial Mission Loadings," *Proceedings of the 8th National Turbine Engine High Cycle Fatigue Conference*, Monterey, CA, 2003.
2. Goodin, E., Kallmeyer, A.R., and Kurath, P., "Evaluation of Nonlinear Cumulative Damage Models for Assessing HCF/LCF Interactions in Multiaxial Loadings," *Proceedings of the 9th National Turbine Engine High Cycle Fatigue Conference*, Pinehurst, NC, 2004.
3. Kallmeyer, A.R., and Kurath, P., "Development of Multiaxial Fatigue Damage Assessment Methods Considering LCF/HCF Interactions," *Final Report*, AFRL Contract No. FA8650-04-1-5211, 2006.
4. Erickson, M., Kallmeyer, A.R., Van Stone, R., and Kurath, P., "Development of a Multiaxial Fatigue Damage Model for High Strength Alloys using a Critical Plane Methodology," *ASME Journal of Engineering Materials and Technology*, Vol. 130, October 2008.
5. Fatemi, A. and Yang, L., "Cumulative Fatigue Damage and Life Prediction Theories: A Survey of the State of the Art for Homogeneous Materials," *Int. J. Fatigue*, Vol. 20, 1998, pp. 9-34.
6. Manson, S.S. and Halford, G.R., "Practical Implementation of the Double Linear Damage Rule and Damage Curve Approach for Treating Cumulative Fatigue Damage," *Int. J. Fatigue*, Vol. 17, 1981, pp. 169-192.
7. Halford, G.R. and Manson, S.S., "Reexamination of Cumulative Fatigue Damage Laws," *Structure Integrity and Durability of Reusable Space Propulsion Systems, NASA CP-2381*, 1985, pp. 139-145.

Appendix

Table 1. Constant Amplitude Fatigue Data

	Input Values								Elastic-Plastic Stresses (Ansys)				
Test Type	ε_{max} (%)	ε_{min} (%)	γ_{max} (%)	γ_{min} (%)	P_{max} (N)	P_{min} (N)	T_{max} (N-m)	T_{min} (N-m)	σ_{max} (MPa)	σ_{min} (MPa)	τ_{max} (MPa)	τ_{min} (MPa)	N
R = 0 Torsion	0.00	0.00	1.31	-0.05					0.00	0.00	425.15	-87.23	1,100,000+
R = 0 Torsion	0.00	0.00	1.75	-0.05					0.00	0.00	465.34	-197.75	118,500
R = 0 Torsion	0.00	0.00	1.56	0.00					0.00	0.00	458.41	-149.35	348,355
R=-1 Torsion	0.00	0.00	0.80	-0.87					0.00	0.00	323.04	-341.70	129,105
R = -1 Torsion	0.00	0.00	1.97	-1.94					0.00	0.00	451.30	-456.81	671
R = 0 Torsion	0.00	0.00	1.92	-0.02					0.00	0.00	462.32	-213.59	19,688
R = 0 Torsion	0.00	0.00	1.72	-0.02					0.00	0.00	468.52	-141.93	36,028
R = 0 Torsion	0.00	0.00	1.42	-0.02					0.00	0.00	441.65	-75.10	982,885
R = -1 Torsion	0.00	0.00	1.03	-1.02					0.00	0.00	382.40	-355.52	16,516
R = -1 Torsion	0.00	0.00	0.85	-0.84					0.00	0.00	331.41	-299.03	68,928
R = -1 Torsion	0.00	0.00	0.75	-0.74					0.00	0.00	283.87	-264.58	1,100,000+
R = -1 Torsion	0.00	0.00	0.85	-0.84					0.00	0.00	312.81	-306.61	190,414
R = 0 Torsion	0.00	0.00	1.81	0.00					0.00	0.00	482.99	-155.71	34,832
R = 0 Torsion							81.29	0.00	0.00	0.00	521.49	-64.39	74,151
R = 0 Torsion							75.64	0.00	0.00	0.00	489.33	-58.18	789,612
R = -1 Torsion							46.85	-46.85	0.00	0.00	334.69	-334.69	200,000
R = -1 Torsion							50.81	-50.81	0.00	0.00	359.71	-359.71	110,404
R = 0 Axial	1.19	-0.34	0.00	0.00					782.04	-697.88	0.00	0.00	9,853
R = 0 Axial	1.51	-0.01	0.00	0.00					828.19	-710.05	0.00	0.00	6,460
R = 0 Axial	0.56	-0.01	0.00	0.00					619.60	0.00	0.00	0.00	3,000,000+
R = 0 Axial	0.58	-0.04	0.00	0.00					657.63	-50.53	0.00	0.00	3,000,000+
R = 0 Axial	0.69	0.00	0.00	0.00					745.02	-36.84	0.00	0.00	135,800
R=0 Axial	1.21	-0.01	0.00	0.00					815.68	-446.49	0.00	0.00	17393
R = -1 Axial	1.27	-1.27	0.00	0.00					701.57	-750.45	0.00	0.00	229
R = -1 Axial	1.26	-1.26	0.00	0.00					824.16	-820.14	0.00	0.00	210
R=0 Proportional					26688.0	0.0	42.9	0.0	647.22	-25.90	299.32	-11.72	997660
R=0 Proportional					22240.0	0.0	62.1	0.0	519.78	-40.93	493.19	-37.13	29644
R=0 Proportional					20016.0	0.0	58.7	0.0	469.67	-35.17	396.71	-29.02	2,000,000+
R=0 Proportional					22240.0	0.0	67.7	0.0	513.17	-46.16	452.56	-37.13	Yielding at 20,000
R=0 Proportional					20460.8	0.0	62.1	0.0	476.29	-39.58	416.99	-33.18	132237

Table 2. Test Data from Multiaxial Mission Histories

Test Type	Input Values								Elastic-Plastic Stresses (Ansys)				N
	ε_{max} (%)	ε_{min} (%)	γ_{max} (%)	γ_{min} (%)	P_{max} (N)	P_{min} (N)	T_{max} (N-m)	T_{min} (N-m)	σ_{max} (Mpa)	σ_{min} (Mpa)	τ_{max} (Mpa)	τ_{min} (Mpa)	
Torsion/Tension Mission	0.00	0.00	1.80	-0.01					-3.03	-3.01	475.44	-261.52	6,780
	0.62	0.01	0.00	0.00					600.81	-6.24	-114.78	-114.78	
Torsion/Proportional Mission	0.00	0.00	1.80	0.00					0.00	0.00	478.24	-257.69	37,286
	0.39	0.00	0.84	0.02					397.87	-28.71	93.08	-247.61	
Torsion/Torsion Mission	0.00	0.00	1.83	0.00					0.00	0.00	478.07	-284.83	11,068
	0.00	0.00	1.32	0.00					0.00	0.00	272.98	-279.61	
Axial/Torsion Mission	0.74	0.02	0.00	0.00					743.77	-0.75	-1.45	-1.45	130,000+
	0.00	0.00	0.92	-0.37					-0.05	-0.04	387.16	-152.55	
Axial/Axial Mission	0.64	-0.06	0.00	0.00					751.24	0.69	0.00	0.00	403,150
	0.51	-0.05	0.00	0.00					616.83	3.45	0.00	0.00	
Torsion/Torsion Mission	0.00	0.00	1.74	0.00					0.00	0.00	446.53	-174.84	9,201
	0.00	0.00	1.23	0.08					0.00	0.00	265.90	-144.87	
Axial/Axial Mission	0.58	-0.11	0.00	0.00					749.87	0.00	0.00	0.00	331,841
	0.46	-0.11	0.00	0.00					689.91	0.00	0.00	0.00	
Torsion/Torsion Mission	0.00	0.00	1.74	0.00					0.00	0.00	446.95	-168.20	9,488
	0.00	0.00	1.12	0.08					0.00	0.00	237.12	-136.87	
Torsion/Torsion Mission	0.00	0.00	1.74	0.00					0.00	0.00	439.95	-161.34	9,920
	0.00	0.00	1.12	0.08					0.00	0.00	233.02	-133.98	
Torsion/Torsion Mission	0.00	0.00	0.89	-0.86					0.00	0.00	311.54	-298.95	3,408
	0.00	0.00	0.61	-0.61					0.00	0.00	216.51	-211.96	
Axial/Axial Mission	1.20	0.00	0.00	0.00					863.28	-404.26	0.00	0.00	9216
	0.59	0.00	0.00	0.00					245.39	-398.85	0.00	0.00	

Table 2 (cont). Test Data from Multiaxial Mission Histories

Test Type	Input Values								Elastic-Plastic Stresses (Ansys)				
	ε_{max} (%)	ε_{min} (%)	γ_{max} (%)	γ_{min} (%)	P_{max} (N)	P_{min} (N)	T_{max} (N-m)	T_{min} (N-m)	σ_{max} (Mpa)	σ_{min} (Mpa)	τ_{max} (Mpa)	τ_{min} (Mpa)	N
					24464.00	0.00	0.00	0.00	596.47	-21.30	-56.26	-56.27	140234
Torsion/Tension Mission					0.00	0.00	81.29	0.00	-8.15	-7.38	520.91	-64.24	16,867
					20460.80	0.00	0.00	0.00	501.21	-15.44	-58.72	-58.72	843,341
Torsion/Proportion Mission					0.00	0.00	81.29	0.00	-0.15	-0.05	521.44	-64.37	9,962
					16012.80	0.00	49.68	0.00	403.87	-0.41	296.16	-64.35	498,051
Torsion/Proportion Mission					0.00	0.00	81.29	0.00	-0.04	-0.01	521.42	-64.37	25,090
					13344.00	0.00	41.77	0.00	336.82	-0.08	238.87	-64.37	1,254,450
Torsion/Torsion Mission					0.00	0.00	81.29	0.00	0.00	0.00	521.42	-64.37	29,958
					0.00	0.00	59.84	0.00	0.00	0.00	369.87	-64.31	1,527,868
Proportional/Axial Mission					20460.80	0.00	62.10	0.00	474.76	-40.80	417.38	-32.73	2,975
					24464.00	0.00	0.00	0.00	576.38	-41.34	-32.44	-32.44	151,714
Proportional/Proportional Mission					20460.80	0.00	62.10	0.00	476.29	-39.58	416.98	-33.18	18,762
					16012.80	0.00	49.68	0.00	364.66	-39.35	327.39	-33.18	956,871
Proportional/Torsion Mission					20460.80	0.00	62.10	0.00	476.62	-39.33	416.82	-33.27	17,161
					0.00	0.00	59.84	0.00	-39.08	-38.94	400.81	-33.38	875,111